

Quantitative Characterization of Critical Nanoclusters Nucleated on Large Single Molecules

Paul M. Winkler,^{1,2,*} Aron Vrtala,¹ Gerhard Steiner,¹ Daniela Wimmer,^{1,5} Hanna Vehkamäki,³ Kari E. J. Lehtinen,⁴
Georg P. Reischl,¹ Markku Kulmala,³ and Paul E. Wagner¹

¹*Fakultät für Physik, Universität Wien, Boltzmannngasse 5, A-1090 Wien, Austria*

²*Advanced Study Program, National Center for Atmospheric Research, Boulder, Colorado, 80305, USA*

³*Department of Physics, University of Helsinki, P.O. Box 64, 00014 University of Helsinki, Finland*

⁴*Department of Applied Physics, University of Eastern Finland and Finnish Meteorological Institute, Kuopio Unit, FIN-70211 Kuopio, Finland*

⁵*Johann Wolfgang Goethe Universität Frankfurt, Institut für Atmosphäre und Umwelt, Altenhöferallee 1, 60438 Frankfurt am Main, Germany*

(Received 17 October 2011; published 23 February 2012)

First order phase transitions involve nucleation, formation of nanoscale regions of a new phase within a metastable parent phase. Using the heterogeneous nucleation theorem we show how clusters formed by nucleation on single molecules evolve from the gas phase and determine the critical size beyond which condensation starts to form aerosol particles. Our experiments reveal the activation of molecules into droplets to happen via formation of critical clusters substantially larger than the seed molecule. The nanosized critical clusters were found to be well predicted by the Kelvin-Thomson relation pointing directly to the key step in the phase transition.

DOI: 10.1103/PhysRevLett.108.085701

PACS numbers: 64.60.Q-, 36.40.-c, 82.70.Rr

Gas-to-particle conversion in air is known to be an important process in atmospheric aerosol formation and cloud microphysics. Particle or droplet formation is always initiated by nucleation occurring either directly in the gas phase (homogeneous nucleation) or on the surface of pre-existing seed particles (heterogeneous nucleation). The latter is energetically much more favorable, resulting in comparatively low vapor supersaturations required for droplet formation. Physicochemical properties of the nucleation sites such as size, solubility, and charging state significantly influence the nucleation process. Nucleation occurs if spontaneously formed clusters reach a critical size allowing the cluster to grow further by condensation. Critical clusters can thus be viewed as the starting point initiating the transition from nanometer sized clusters into macroscopically relevant objects like cloud condensation nuclei and cloud droplets. The importance of quantifying critical nuclei in size and chemical composition was highlighted recently in the context of atmospheric particle formation [1].

Modeling nucleation suffers from the fact that on the one hand cluster dimensions often exceed the applicability range of quantum mechanical approaches and on the other hand they are too small to be modeled accurately by macroscopic theories. This unsatisfying situation is underlined by recent experimental studies reporting nanoparticle activation at sizes much smaller than expected from thermodynamically derived vapor-droplet equilibrium conditions [2,3]. It is notable that we can now analyze experimental nucleation data independent of any theoretical model by applying the nucleation theorems for homogeneous [4,5] and heterogeneous [6] nucleation to obtain

the number of molecules in a critical cluster. In this Letter, we present precision heterogeneous nucleation experiments which have been analyzed with the recently developed heterogeneous nucleation theorem to determine the size of critical clusters formed on preexisting nucleation sites. We investigated the activation behavior of single ion molecules in supersaturated *n*-propanol vapor and determined the number of molecules in the critical clusters from heterogeneous nucleation probability vs saturation ratio curves. The challenging aspects as well as the novelty of this work are related to the experimental precautions undertaken to allow for the direct application of the heterogeneous nucleation theorem to experimental data. Any extra factors influencing the slope of heterogeneous nucleation probability curves need to be eliminated in order to achieve meaningful results. This requires precise settings of the thermodynamic state and strictly monodisperse seed particles as was pointed out recently [7].

Heterogeneous nucleation on single ion molecules was investigated at two different temperatures using an expansion chamber in combination with an optical particle detection system (constant angle Mie scattering, CAMS method [8]). Details of the experimental system can be found elsewhere [9,10]. *n*-Propanol vapor was added to the system by controlled injection from a syringe pump and mixed with a well-defined flow of size selected positive or negative ion molecules with diameters between 1.47 and 1.78 nm. Ion molecules were generated by electrospray ionization [11] in combination with a high resolution electrostatic size classifier [12]. Further experimental details can be found in [13]. The size of the ion molecules was determined from electrical mobilities according to Ude and

de la Mora [14]. Vapor supersaturation was achieved by adiabatic expansion and number concentration of droplets nucleated on ion molecules was measured by the CAMS detector. For each n -propanol vapor saturation ratio, the fraction of activated particles relative to total particle number concentration was determined at different temperatures, resulting in temperature dependent nucleation probability curves for each of the investigated ion molecules (see Fig. 2).

The key issue in this study was to identify and use seed particles of strictly monodisperse size since any finite distribution of particle sizes leads to a flattening of heterogeneous nucleation probability curves and hence underestimation of critical cluster sizes. We chose ion molecules of particular species, which can be regarded as perfectly monodisperse seed particles. In the present study, positive tetraheptylammoniumbromide (monomer THA^+ and dimer THA_2^+Br) and tetradodecylammoniumbromide (monomer TDDA^+ and dimer THABr_2^-) were used. In Fig. 1 size distributions of the corresponding ions are illustrated. The remaining measured widths of the peaks are below a relative full width at half maximum (FWHM) of 3% and can be attributed to the nonideal transfer function of the electrostatic classifier. The mobility classified sizes of these ions were found to be 1.47, 1.78, 1.70, and 1.54 nm for THA^+ , THA_2^+Br , TDDA^+ and THABr_2^- , respectively, (see also Table I). These substances were described in detail earlier as mass and mobility standards [14]. In Fig. 2 the temperature dependence of heterogeneous nucleation probability curves is shown for selected ions. As can be seen, with decreasing temperature as well as decreasing ion molecule size the saturation ratio required to activate the ion molecules is increased.

Quantitative information on critical cluster size is obtained from the heterogeneous nucleation theorem for charged particles [15],

$$\left. \frac{\partial \ln(\ln \frac{1}{1-P})}{\partial \ln S} \right|_T = \Delta N_2^* - \Delta N_1^*, \quad (1)$$

where P and S denote heterogeneous nucleation probability and vapor saturation ratio, T is temperature, while ΔN_1^* and ΔN_2^* are the excess numbers of molecules in a stable prenucleation cluster and the critical cluster, respectively. Excess number is the number of molecules in the cluster

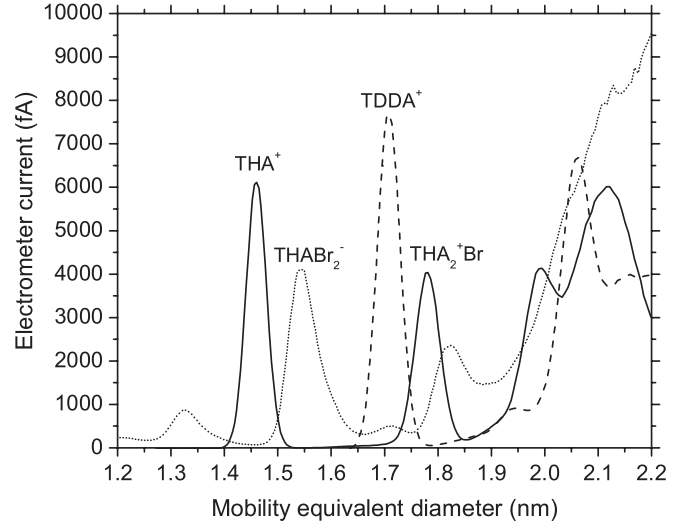


FIG. 1. Size distributions of THA^+Br (solid) and TDDA^+Br (dashed) ions as well as THABr_2^- (dotted) as determined with the nano-DMPS.

minus the number that would occupy the cluster volume if filled with vapor phase. Liquid being much denser than the vapor, ΔN_2^* is fairly accurately equal to the number of molecules in the cluster. ΔN_1^* needs to be considered in Eq. (1) only if stable prenucleation clusters will actually be formed in the considered system. To illustrate this issue, Fig. 3 shows the formation free energy curves as a function of number of n -propanol molecules in the cluster. Classical nucleation theory for homogeneous and ion-induced nucleation (with zero contact angle) has been used to create these curves. The formation free energies have been made self-consistent [16] so that the formation free energy of the monomer (number of molecules $N = 1$) in the case of homogeneous nucleation and a bare ion ($N = 0$) in the case of ion-induced nucleation have been set to zero. The resulting form for the homogeneous formation free energy is

$$\Delta G(N) = -(N - 1)kT \ln S + [A(N) - A(1)]\sigma \quad (2)$$

and for the ion-induced free energy

$$\Delta G(N) = -NkT \ln S + [A(N) - A(0)]\sigma + \frac{q^2}{8\pi\epsilon_0} \left(1 - \frac{1}{\epsilon_r}\right) \left(\frac{1}{r(N)} - \frac{1}{r(0)}\right). \quad (3)$$

TABLE I. Physicochemical properties of seed ion molecules and critical clusters. ΔN_1^* and ΔN_2^* are the excess numbers of molecules in a stable prenucleation cluster and the critical cluster, respectively.

Seed ion molecule	Chemical formula	Atomic mass (Da)	Mobility diameter (nm)	$\Delta N_2^* - \Delta N_1^*$ (273 K)	$\Delta N_2^* - \Delta N_1^*$ (263 K)
THA^+ monomer	$(\text{C}_7\text{H}_{15})_4\text{N}^+$	410.78	1.47	47^{+19}_{-8}	42^{+21}_{-11}
THA_2^+Br dimer	$[(\text{C}_7\text{H}_{15})_4\text{N}]_2^+\text{Br}$	901.46	1.78	48^{+26}_{-7}	44^{+26}_{-13}
THABr_2^- dimer	$(\text{C}_7\text{H}_{15})_4\text{NBr}_2^-$	584.60	1.54	50^{+10}_{-6}	37^{+7}_{-4}
TDDA^+	$(\text{C}_{12}\text{H}_{25})_4\text{N}^+$	691.31	1.70	56^{+29}_{-13}	53^{+28}_{-12}

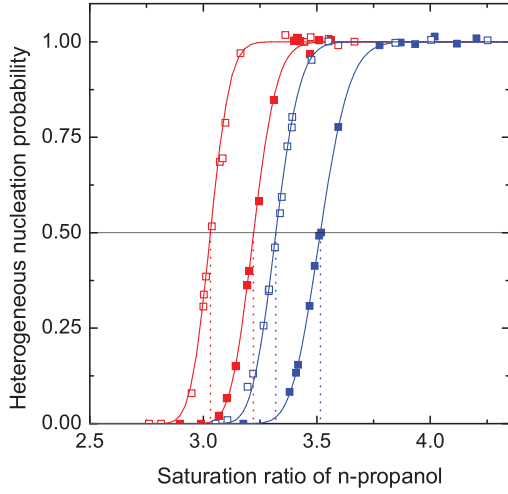


FIG. 2 (color). Heterogeneous nucleation probability P vs vapor saturation ratio for nucleation of n -propanol on THA^+Br ions at 273 K (red) and 263 K (blue). Open squares refer to the dimer with mobility diameter 1.78 nm and full squares to the monomer with 1.47 nm. Lines are fitted to the data according to physically consistent heterogeneous nucleation probability functions. Corresponding onset saturation ratios ($P = 0.5$) are indicated by vertical dotted lines.

In these equations σ is the “bulk” surface tension (for flat surfaces), $r(N)$ and $A(N)$ are the radius and surface area of a N cluster, q is the charge of the ion, ϵ_r is the (bulk liquid) dielectric constant of the formed n -propanol cluster and ϵ_0 permittivity of vacuum. The homogeneous formation free energy curve (Fig. 3) does not contain a minimum, and thus the process does not involve stable prenucleation clusters. The ion-induced formation free energy with an ion radius 0.1 nm has a minimum followed by a maximum, corresponding to the occurrence of a prenucleation cluster and critical clusters, respectively. The curve with an ion radius 0.9 nm has no minimum, and thus no stable prenucleation clusters are formed on an ion of this size (assuming a zero contact angle).

For practical reasons we applied the heterogeneous nucleation theorem to physically consistent fit functions determined from the experimental data [13]. In Table I, $\Delta N_2^* - \Delta N_1^*$ including uncertainty ranges are given for the different seed ion molecules and two temperatures at the onset saturation ratio, i.e., the saturation ratio where $P = 0.5$.

The condition for critical cluster (prenucleation cluster) in unstable (stable) equilibrium with the surrounding vapor is found by locating the maximum (or minimum) of the formation free energies (2) and (3). The conditions are given by Kelvin equation

$$kT \ln S = \frac{2\sigma M}{N_A \rho r} \quad (4)$$

for neutral particles and Kelvin-Thomson (K-T) equation [17]

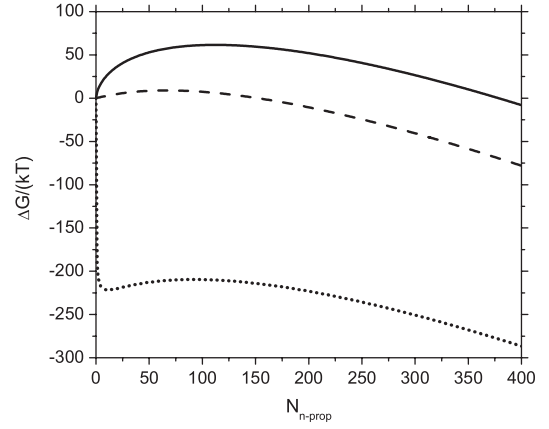


FIG. 3. Formation free energies for homogeneous nucleation (solid line) and ion-induced nucleation of n -propanol ($S = 3.0$, $T = 273.15$ K) at two different ion sizes (dashed line is calculated for ion radius 0.9 nm, dotted line for ion radius 0.1 nm). Prenucleation clusters are expected to form only when the energy curves go through a minimum as is the case for an ion with radius 0.1 nm.

$$kT \ln S = \frac{2\sigma M}{N_A \rho r} - \frac{q^2 M}{8\pi \epsilon_0 N_A \rho r^4} \left(1 - \frac{1}{\epsilon_r}\right) \quad (5)$$

for charged particles. Here M and ρ denote molecular weight and (liquid) density of the condensate and N_A is Avogadro’s number. For thermodynamic data used see Table S1 in [13]. The vapor saturation ratio determines the curvature of the equilibrium cluster surface, and thus the cluster radius. In the case of heterogeneous nucleation, the critical cluster is located upon the seed particle, and the number of molecules is related to the radius through a geometric relation involving contact angle. The contact angle describes the interaction between the cluster molecules and the seed particle (wetting ability) and it can depend on the radius of the cluster [18]. Under the assumption of complete wetting (contact angle 0°) the volume of the seed particle fully contributes to the critical cluster volume and correspondingly the curvature of the surface of a cluster containing a certain number of molecules can be directly determined. Thereby, the volume of the critical cluster V_{crit} can be calculated according to

$$V_{\text{crit}} = V_{\text{seed}} + \Delta N_2^* V_{n\text{-prop}}^l, \quad (6)$$

where V_{seed} is the volume of the seed particle and $V_{n\text{-prop}}^l$ the volume of one n -propanol molecule in bulk liquid. For spherical critical clusters the diameter d_{crit} is calculated from

$$d_{\text{crit}} = \sqrt[3]{\frac{6V_{\text{crit}}}{\pi}}. \quad (7)$$

In Fig. 4, the initial seed ion molecule size and the size of the critical cluster together with corresponding values according to the classical K-T equation are shown for

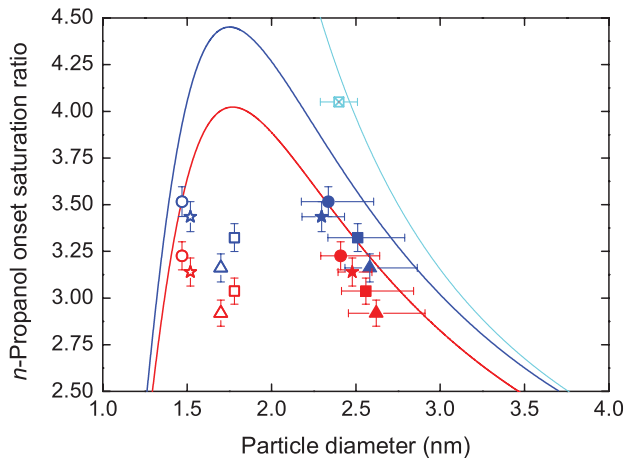


FIG. 4 (color). Experimental onset saturation ratios measured at 273 K (red) and 263 K (blue) as function of seed particle mobility diameter for ions (open symbols) together with the diameter of the corresponding critical cluster (full symbols). Circles refer to THA^+ monomer, squares to THA_2^+Br dimer, triangles to TDDA^+ and stars to THABr_2^- dimer. Solid lines indicate the prediction of the Kelvin-Thomson equation at 273 K (red) and 263 K (blue). Horizontal error bars were obtained by means of variation analysis and indicate the possible range of critical clusters. Vertical error bars show experimental uncertainty in saturation ratio (typically below 2% of absolute value). For comparison the agreement of homogeneous nucleation data and Kelvin equation is shown for 265 K (cyan).

263 and 273 K. For simplicity, we show the critical cluster diameters assuming that there are no prenucleation clusters ($\Delta N_1^* = 0$) as suggested by the classical theory for ions of studied size. The purely experimentally determined error bars indicate remarkably good agreement of our data with K-T equation spanning entirely the range of uncertainty given by a possible adsorbed monomolecular layer. The sizes of the critical clusters as plotted in Fig. 4 can thus be viewed as the minimum sizes possible under complete wetting. On the other hand, by considering only $V_{\text{seed}}/2$ in Eq. (6) it can be quantitatively shown that a significant effect of a nonzero contact angle on the critical cluster size can be ruled out. This is a consequence of the fact that the final critical cluster is substantially larger than the initial seed molecule. Accordingly, the bulk values used for surface tension and dielectric constant to compute K-T equation represent reasonable approximations in our study where the bare ion is covered by substantially more condensate than just a monolayer. Similarly, a recent theoretical nucleation study [19] has found little effects of a Tolman-type corrected surface tension compared to the surface tension of a plane surface.

It is important to note that activation behaviors of different seed molecules (TDDA^+Br) and molecules with different polarity (THABr_2^-) do not follow the size dependence of the THA^+Br molecules indicating different nucleation behavior. However, the critical clusters (full symbols) are

approximately in line as expected from the K-T prediction. One of the major shortcomings attributed to the classical K-T equation is related to the fact that this equation does not allow to differentiate between positive and negative polarities [20]. Here we show, however, that K-T provides a rather precise tool to determine critical cluster sizes regardless of the properties of the individual seed particles. Notably, the experimentally observed temperature dependence is within error exactly in accordance with K-T equation. From Fig. 4 it becomes clear that the nucleating molecules forming a critical cluster are shifting the size of the initial seed particle towards the Kelvin-Thomson diameter providing the curvature for which the vapor is in equilibrium. This formation of critical clusters with diameters given by the Kelvin-Thomson equation is observed regardless of the actual properties of the particular seed particles. Further addition of a single vapor molecule by statistical fluctuation causes the critical cluster to grow immediately by condensation. Thereby the initial seed molecule becomes visible and hence detectable by optical methods. We would like to emphasize that all our evaluations are independent of classical/macroscopic assumptions with the only exception that we assume macroscopic liquid density in the critical cluster. Departure of cluster density from the macroscopic value towards smaller densities would even improve agreement between experimental data and K-T. Figure 4 also illustrates homogeneous nucleation data in comparison to Kelvin equation at 265 K [21]. The agreement of critical cluster size in homogeneous nucleation with Kelvin was also found with other compounds [22,23].

While the Kelvin-Thomson prediction is within the uncertainty limits of our experiments, it tends to slightly overestimate the experimental critical cluster sizes by roughly 15–20 molecules. This can probably be interpreted by a recently derived modification of the classical Kelvin-Thomson equation. Taking into account effects of the central electric field and the disjoining pressure on condensing thin liquid films [24] leads to a reduction of the nucleation barrier and correspondingly to lower saturation ratios required to achieve critical cluster formation. Our results clearly support the macroscopic Kelvin or Kelvin-Thomson theory being able to describe vapor equilibrium conditions for critical clusters with diameters as small as a few nanometers. However, the classical nucleation theory often fails to explain experimental heterogeneous nucleation data quantitatively. Our data thus support the recent theoretical study [25] which has demonstrated that the Kelvin equation is more fundamental than classical nucleation theory.

The results of our experiments indicate that the size of the critical cluster agrees quite well with the Kelvin or Kelvin-Thomson prediction, although the initial seed is substantially smaller (see schematic illustration in Fig. S1 [13]). Until recently it has been widely accepted

that seed particles need to be larger than the Kelvin or Kelvin-Thomson radius in order to be activated. This would be the case if particles only activated for growth when the nucleation barrier vanishes and (barrierless) condensation occurs. However, this ignores the fact that a nucleation barrier can be crossed by kinetic processes, and hence also smaller particles can activate for growth via heterogeneous or ion-induced nucleation. As a consequence, our data quantitatively indicate a considerable extension of the fundamental detection range of condensation particle counters (CPCs) down to nanoparticles or subnanoparticles or even single molecules which is of great practical importance [26–28].

The clustering of initially gas-phase molecules transitioning into bulk liquid phase material takes place within a narrow range of molecule numbers. In their pioneering work on gas-phase clusters more than two decades ago, Castleman and Keesee [29] raised the question how large a cluster needs to be until it displays properties of the macroscopic bulk phase. We now have obtained clear experimental evidence that critical clusters with radii down to about 2 nm are satisfactorily described by the (macroscopic) Kelvin or Kelvin-Thomson relation. This will give new firm insight to nucleation and initial growth processes in atmospheric conditions as well improve our understanding of nanomaterials.

This work was supported by the Austrian Science Fund (FWF): [P19546-N20], [P20837-N20], [L593-N20] and [J3198-N21], the Academy of Finland (Center of Excellence program project number 1118615, LASTU program project number 135054) and ERC projects 257360-MOCAPAF and 27463-ATMNUCLE. The National Center for Atmospheric Research is supported by the National Science Foundation. We also appreciate the help of Dr. Jan Wedekind for providing the homogeneous nucleation data point in Fig. 4.

*Corresponding author.
pwinkler@ucar.edu

- [1] R. Zhang, *Science* **328**, 1366 (2010).
- [2] M. Gamero-Castaño and J. F. de la Mora, *J. Chem. Phys.* **117**, 3345 (2002).
- [3] P. M. Winkler *et al.*, *Science* **319**, 1374 (2008).
- [4] D. W. Oxtoby and D. Kashchiev, *J. Chem. Phys.* **100**, 7665 (1994).

- [5] D. Kashchiev, *Nucleation: Basic Theory with Applications* (Butterworth-Heinemann, Oxford, 2000).
- [6] H. Vehkamäki *et al.*, *J. Chem. Phys.* **126**, 174707 (2007).
- [7] J. Fernandez de la Mora, *Aerosol Sci. Technol.* **45**, 543 (2011).
- [8] P. E. Wagner, *J. Colloid Interface Sci.* **105**, 456 (1985).
- [9] P. M. Winkler, A. Vrtala, and P. E. Wagner, *Atmos. Res.* **90**, 125 (2008).
- [10] P. E. Wagner, D. Kaller, A. Vrtala, A. Lauri, M. Kulmala, and A. Laaksonen, *Phys. Rev. E* **67**, 021605 (2003).
- [11] L. de Juan and J. F. de la Mora, *J. Colloid Interface Sci.* **186**, 280 (1997).
- [12] G. Steiner, M. Attoui, D. Wimmer, and G. P. Reischl, *Aerosol Sci. Technol.* **44**, 308 (2010).
- [13] See Supplemental Material at <http://link.aps.org/supplemental/10.1103/PhysRevLett.108.085701> for details and procedures.
- [14] S. Ude and J. F. de la Mora, *J. Aerosol Sci.* **36**, 1224 (2005).
- [15] H. Vehkamäki, M. J. McGrath, T. Kurtén, J. Julin, K. E. J. Lehtinen, and M. Kulmala, *J. Chem. Phys.* (to be published).
- [16] S. L. Girshick and C.-P. Chiu, *J. Chem. Phys.* **93**, 1273 (1990).
- [17] J. J. Thomson, *Conduction of Electricity through Gases* (Cambridge University Press, London, 1906).
- [18] A. I. Hienola *et al.*, *J. Chem. Phys.* **126**, 094705 (2007).
- [19] M. Schrader, P. Virnau, and K. Binder, *Phys. Rev. E* **79**, 061104 (2009).
- [20] A. B. Nadykto, J. M. Mäkelä, F. Yu, M. Kulmala, and A. Laaksonen, *Chem. Phys. Lett.* **382**, 6 (2003).
- [21] A. Manka, J. Wedekind, D. Ghosh, K. Iland, J. Wölk, and R. Strey, *J. Chem. Phys.* (to be published).
- [22] R. Strey, P. E. Wagner, and Y. Viisanen, *J. Phys. Chem.* **98**, 7748 (1994).
- [23] Y. J. Kim, B. E. Wyslouzil, G. Wilemski, J. Wölk, and R. Strey, *J. Phys. Chem. A* **108**, 4365 (2004).
- [24] A. K. Shchekin and T. S. Podguzova, *Atmos. Res.* **101**, 493 (2011).
- [25] R. McGraw and E. R. Lewis, *J. Chem. Phys.* **131**, 194705 (2009).
- [26] K. Iida, M. R. Stolzenburg, and P. H. McMurry, *Aerosol Sci. Technol.* **43**, 81 (2009).
- [27] L. A. Sgro and J. Fernandez de la Mora, *Aerosol Sci. Technol.* **38**, 1 (2004).
- [28] J. Vanhanen *et al.*, *Aerosol Sci. Technol.* **45**, 533 (2011).
- [29] A. W. Castleman and R. G. Keesee, *Science* **241**, 36 (1988).